Journal of Alloys and Compounds 509 (2011) 8880–8884

Contents lists available at ScienceDirect

Journal of Alloys and Compounds

journal homepage: www.elsevier.com/locate/jallcom

Optical spectra and excited state relaxation dynamics of Nd^{3+} in CaF_2 single crystal

Qingguo Wang[a,b], Liangbi Su[a,*], Hongjun Li[a], Lihe Zheng[a], Xin Guo[a,b], Dapeng Jiang[a,b], Hengyu Zhao[a], Jun Xu[a,*], Witold Ryba-Romanowski[c], Piotr Solarz[c], Radoslaw Lisiecki[c]

[a] Key Laboratory of Transparent and Opto-Functional Advanced Inorganic Materials, Shanghai Institute of Ceramics, Chinese Academy of Sciences, Shanghai 201800, People's Republic of China
[b] Graduate School of the Chinese Academy of Science, Beijing 100039, People's Republic of China
[c] Institute of Low Temperature and Structure Research, Polish Academy of Sciences (ILTSR), Okolna 2, 50-422 Wroclaw, Poland

ARTICLE INFO

Article history:
Received 17 March 2011
Received in revised form 3 May 2011
Accepted 5 May 2011
Available online 8 July 2011

Keywords:
Nd-doped CaF_2
TGT method
Low-temperature optical spectra
Judd–Ofelt theory

ABSTRACT

Nd-doped CaF_2 crystal with high optical quality was obtained by a temperature gradient technique (TGT). Energies of the crystal field levels of Nd^{3+} multiplets relevant to laser operation were determined based on optical spectra recorded at $T = 10$ K. Room temperature absorption spectra were analyzed in the framework of the Judd–Ofelt theory to calculate radiative transition rates and luminescence branching ratios for the $^4F_{3/2}$ level. The $^4F_{3/2}$ radiative lifetime was calculated to be 1295 μs whereas a monotonous decrease of the $^4F_{3/2}$ luminescence lifetime value from 1.45 ms to 0.9 ms was observed when the temperature increased from 10 K to 300 K. The stimulated emission cross-section of 1.48×10^{-20} cm^2 at 1061 nm was determined using the Fuchtbauer–Ladenburg relation. All the results showed that Nd:CaF_2 would be a promising gain media in solid-state lasers.

1. Introduction

Early studies of rare earth-doped CaF_2 crystals have been reported in the sixties of the past century already [1–4]. Subsequent interest in these systems was rather small because the requirement of the charge compensation has been considered as a major drawback. More recent works have been aimed at the understanding of the nature of numerous non equivalent rare earth ion centers. Considerable attention has been paid to neodymium-doped CaF_2. The laser-selective-excitation studies of hydrogenated CaF_2:Nd^{3+} crystals have identified numerous F-charge compensated centers in addition to well established C_{4V} centers [5,6]. Site selective and time resolved spectroscopy has been applied to determine level splitting and nonradiative relaxation of aggregated centers in Nd^{3+}-doped CaF_2 [7–10]. As far as we know, only one published paper has been devoted to the assessment of laser potential of Nd^{3+}-doped CaF_2 system [11]. Authors have performed an analysis of room temperature absorption spectra in the framework of the Judd–Ofelt theory and have determined radiative transition rates and luminescence branching ratios for the $^4F_{3/2}$ emission. Unfortunately, the evaluated $^4F_{3/2}$ radiative lifetime of 199 μs was five times lower than the luminescence lifetime measured [11].

Recently, an interest in the CaF_2 crystal as a host for rare earth ions has been renewed. The scintillation properties of CaF_2:Nd^{3+} crystals were studied in Ref. [12]. CaF_2:Yb^{3+},Er^{3+} nanoparticles and single crystals were synthesized. The upconversion and Near Infrared fluorescence spectra have been analyzed, and the upconversion mechanism has been proposed [13,14]. Yb:CaF_2 system has been identified as a promising laser-diode pumped active material for the design of femtosecond lasers and large scale DPSS lasers owing to broad spectral bands, long luminescence lifetime and reasonably high thermal conductivity [15,16]. Full color photoluminescence combining blue, green and orange-red light was realized by ultraviolet light excitation in Tb^{3+}/Sm^{3+}-codoped SiO_2–Al_2O_3–CaO–CaF_2 glass and glass ceramics systems [17]. Later, CaF_2:Tb,Sm was used as a thermoluminescence dosimeter to measure the daily UV radiant energy in the human mouth successfully [18]. Cooperative downconversion was realized in glass ceramics containing Eu^{2+}/Yb^{3+}:CaF_2 nanocrystals with Eu^{2+} greatly absorbing ultraviolet photons [19]. And the spectroscopic properties of Eu doped CaF_2 ceramics at different concentration were researched by Samuel et al. [20]. The clustering was characterized by the cross-relaxation for Tm:CaF_2 system. A pair model taking into account clustering has been developed [21].

* Corresponding authors.
E-mail addresses: Su_lb@163.com (L. Su), xujun@mail.shcnc.ac.cn (J. Xu).

0925-8388/$ – see front matter © 2011 Elsevier B.V. All rights reserved.
doi:10.1016/j.jallcom.2011.05.022

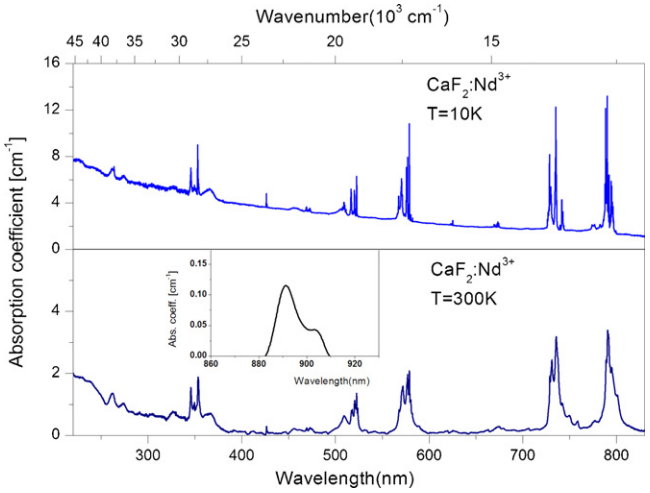

Fig. 1. The absorption spectra of CaF_2:0.75 wt% Nd^{3+} crystal recorded at 10 K and 300 K. Inset shows the absorption band related to the $^4I_{9/2} \rightarrow {}^4F_{3/2}$ transition.

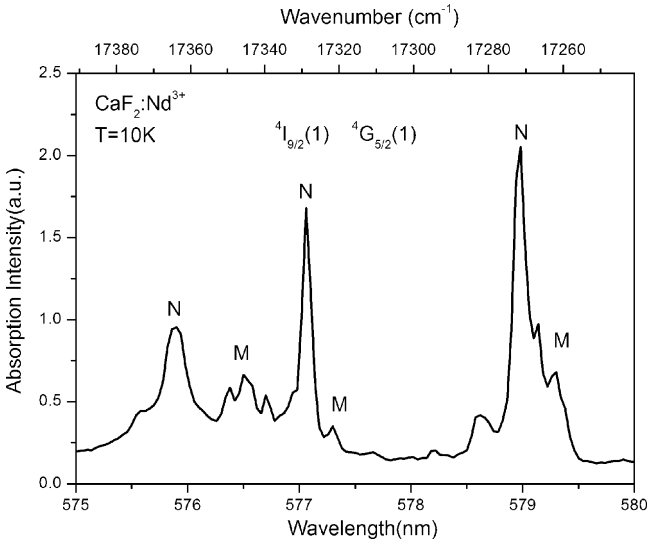

Fig. 2. Absorption spectra of the M and N-type Nd^{3+} centers in CaF_2 crystal in the $^4I_{9/2}(1) \rightarrow {}^4G_{5/2}(1)$ transition at 10 K.

Nanostructured CaF_2:Tm ceramics was confirmed to be a potential gain media for two micro lasers [22]. The potential applications of Pr^{3+}-doped CaF_2 crystal to tunable and picosecond laser operation were studied in Ref. [23]. Among other important advantages the ease of production of CaF_2 nanocrystals and feasibility of manufacturing transparent ceramics are stressed [24–27].

Encouraged by the above arguments we examine in the present work optical features of neodymium-doped CaF_2 crystal aiming at the determination of fundamental spectroscopic parameters relevant to the laser performance of the CaF_2:Nd^{3+} system.

2. Experimental

The raw materials with their purities in parentheses were CaF_2 (99.99%) and NdF_3 (99.99%). The raw powders were mixed to obtain the CaF_2 crystal with intentional 0.92 wt% Nd^{3+} concentration and put into the sealed graphite crucible. The mixtures were melted at 1400 °C, and then grown on the ⟨1 1 1⟩ CaF_2 seeds with reducing the temperature. The cooling rate was about 10 °C/h. The concentration of Nd^{3+} in the crystal grown was measured to be 0.75 wt% by inductively coupled plasma atomic emission spectroscopy (ICP-AES) analysis, pointing at the segregation coefficient for Nd^{3+} ions of about 0.82. The Nd:CaF_2 sample with the thickness of 4.0 mm was prepared and polished for spectroscopic study. Absorption spectra were recorded with a Varian Modal 5E UV–VIS-NIR (UV–visible-near-IR) absorption spectrophotometer at 10 K and 300 K. The spectral bandwidth of the spectrophotometer was set to 0.1 nm in the UV–VIS region and to 0.2 nm in the NIR region. The emission spectra at room temperature and at 10 K were excited by an Argon ion laser at 514 nm and recorded with a Dongwoo Optron monochromator DM 711 with 750 mm focal length, coupled with an infrared detector InGaAs. For low temperature measurement the sample was put into an Oxford Model CF 1204 continuous liquid helium cryostat equipped with a temperature controller.

3. Results and discussion

3.1. Analysis of absorption spectra

Survey absorption spectra recorded at 300 K and at 10 K for the Nd-doped CaF_2 crystal are compared in Fig. 1. Significant broadening of Nd^{3+} absorption bands stems from a certain structural disorder in the doped crystal as a consequence of the disparity in ionic radii and oxidation states of calcium and neodymium ions. It has been shown in the past that upon substitution of Ca^{2+} ions in the CaF_2 crystal lattice by Nd^{3+} ions a number of Nd^{3+} sites with different site symmetries such as O_h, C_{4v} and C_{3v} can be found [28]. In addition, different clusters containing interstitial fluorine F_i^- have been also observed [5]. At 10 K, the absorption transitions originate from the lowest crystal field component of the $^4I_{9/2}$ ground state of Nd^{3+} ions, and the absorption bands show rich structure.

As an example, Fig. 2 presents details of the 10 K absorption band related to the transition between the lowest crystal field levels of the ground $^4I_{9/2}$ and excited $^4G_{5/2}$ states of Nd^{3+} in CaF_2 crystal. Assignment of the band components follows the analysis of the spectra and notation proposed in [7]. The M and N centers are the rhombic $(Nd^{3+}–F^-_i)_2$ dimer clusters and trigonal $(Nd^{3+}–F^-_i)_4$ tetramer clusters formed through the mutual attraction of the $Nd^{3+}–F^-_i$ dipoles. It can be seen from the figure that the absorption associated with N centers dominates in this crystal.

Two features of absorption spectra shown in Fig. 1 are worth our attention. First, the absorption band related to the $^4I_{9/2} \rightarrow {}^4F_{5/2}$ transition near 800 nm is advantageously broad thus offering a possibility of optical pumping with AlGaAs laser diodes without a stringent control of the laser diode temperature. In addition, the band intensity is relatively high. The peak absorption coefficient of the $^4I_{9/2} \rightarrow {}^4F_{5/2}$ transition at 300 K amounts to 3.33 cm^{-1} and the corresponding peak absorption cross-section is 0.75×10^{-20} cm^2 at 791 nm a value comparable to 0.79×10^{-20} cm^2 at 796 nm reported for Nd:SrF_2 crystal [28]. Second, an uncommonly small intensity of the $^4I_{9/2} \rightarrow {}^4F_{3/2}$ transition implies a very long lifetime of the $^4F_{3/2}$ upper laser level, see inset in Fig. 1.

Room temperature absorption spectrum of the grown crystal was analyzed in the framework of the Judd–Ofelt theory [29,30] to determine radiative transition rates and luminescence branching ratios for the $^4F_{3/2}$ metastable level. The similar analysis of Nd-doped CaF_2 crystals and nanocrystals contained in oxyfluoride glass ceramics can be found in Ref. [11,31,32].

Experimental oscillator strengths f_{exp} evaluated by a numerical integration of absorption bands shown in Fig. 1 were used as input data for the calculations. And it can be determined as

$$f_{\mathrm{exp}} = \frac{2m_e c}{\alpha_f h N_0 \lambda^2} \int \alpha(\lambda) d\lambda \quad (1)$$

where α_f is the fine structure constant, N_0 is the number of active ions per unit volume, λ is the average wavelength of the transition, c is the velocity of the light, h is the Planck constant, m_e is the mass of the electron and $\alpha(\lambda)$ is the absorption coefficient.

Expressions for theoretical oscillator strengths f_{theor} were constructed using the reduced matrix elements from Ref. [31].

$$f_{\mathrm{theor}} = \frac{8\pi^2 m_e c}{3h\lambda(2J+1)} \times \frac{1}{n} \times \left[\frac{(n^2+2)^2}{9}\right] \times S_{ed} \quad (2)$$

Table 1
Measured and calculated oscillator strengths for Nd^{3+} in CaF_2.

Transitions from the $^4I_{9/2}$ to levels indicated	Mean wavelength of the transition [nm]	Oscillator strength f_{exp} [10^{-6}]	Oscillator strength f_{theor} [10^{-6}]
$^4F_{3/2}$	896	0.02	0.015
$^4F_{5/2} + {}^2H(2)_{9/2}$	787	1.42	1.43
$^4F_{7/2} + {}^4S_{3/2}$	741	1.46	1.56
$^4F_{9/2}$	679	0.10	0.11
$^2H_{11/2}$	627	0.03	0.03
$^4G_{5/2} + {}^2G(1)_{7/2}$	576	1.64	1.66
$^2K_{13/2} + {}^4G_{7/2} + {}^4G_{9/2}$	511	1.13	1.08
$^2K_{15/2} + {}^2G(1)_{9/2} + {}^2D(1)_{3/2} + {}^4G_{11/2}$	473	0.09	0.12
$^2P_{1/2}$	427	0.39	0.59

$\Omega_2 = 0.31 \times 10^{-20}\ cm^2$; $\Omega_4 = 0.51 \times 10^{-20}\ cm^2$; $\Omega_6 = 1.24 \times 10^{-20}\ cm^2$; RMS = 9.48×10^{-8}.

$$S_{ed}(SLJ \rightarrow S'L'J') = \sum_{t=2,4,6} \Omega_t |\langle SLJ||U^{(t)}||S'L'J'\rangle|^2 \quad (3)$$

where Ω_t (t = 2,4,6) are the Judd–Ofelt parameters which can be obtained by fitting the experimental oscillator strength to the calculated oscillator strength using the least square technique, (S, L, J) are the quantum numbers corresponding to the total spin, total orbit and the total angular momentum, respectively, $U^{(t)}$ are the reduced matrix elements which do not vary with different hosts, and S_{ed} is the calculated electronic dipole transition line strength between two different J states.

The root mean square deviation (RMS) between the experimental and the theoretic calculated values is given by

$$RMS = \left[\sum_i \frac{(f_{theor} - f_{exp})^2}{N - P}\right]^{1/2} \quad (4)$$

where N is the number of the absorption transitions, P is the number of fitted parameters. Results of the fitting procedure are given in Table 1. There is a very large dissimilarity between our intensity parameters and the values $\Omega_2 = 0.87 \times 10^{-20}\ cm^2$, $\Omega_4 = 3.44 \times 10^{-20}\ cm^2$ and $\Omega_6 = 9.47 \times 10^{-20}\ cm^2$ reported earlier in Ref. [11].

With the intensity parameters $\Omega_{2,4,6}$ determined, the radiative transition rates W_r, luminescence branching ratios β and radiative lifetime τ_{rad} for the $^4F_{3/2}$ level were calculated and gathered in Table 2. The expressions used are listed as follows

$$W_r(SLJ \rightarrow S'L'J') = \frac{64\pi^4 e^2}{3h\lambda^3(2J+1)} \times \left[\frac{n(n^2+2)^2}{9} S_{ed} + n^3 S_{md}\right] \quad (5)$$

$$\beta(SLJ \rightarrow S'L'J') = \frac{W_r(SLJ \rightarrow S'L'J')}{\sum_{S'L'J'} W_r(SLJ \rightarrow S'L'J')} \quad (6)$$

$$\tau_{rad} = [W_r(SLJ \rightarrow S'L'J')]^{-1} \quad (7)$$

where S_{md} is the line strength for a magnetic dipole transition. In general, S_{md} is much smaller than S_{ed}, and it can be neglected.Defined as an inverse of the sum of radiative transition rates, the $^4F_{3/2}$ radiative lifetime of the grown crystal was found to be 1295 μs.

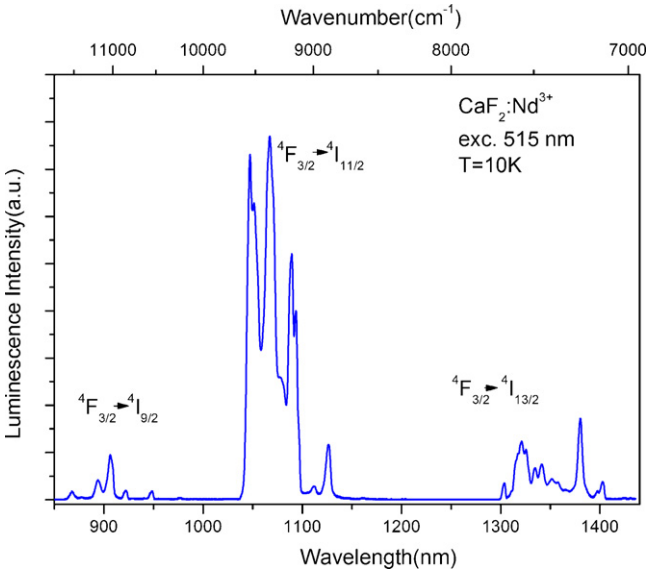

Fig. 3. The NIR luminescence spectrum of Nd:CaF_2 crystal recorded at 10 K.

3.2. Luminescence spectra and excited state relaxation dynamics

The NIR luminescence spectrum of Nd:CaF_2 crystal recorded at 10 K is shown in Fig. 3. The emission bands at 850–950 nm, 1000–1150 nm and 1300–1400 nm correspond to the $^4F_{3/2} \rightarrow {}^4I_{9/2}$, $^4F_{3/2} \rightarrow {}^4I_{11/2}$ and $^4F_{3/2} \rightarrow {}^4I_{13/2}$ transitions, respectively. The emission bands are well resolved and make it possible to locate easily the crystal field components of the terminal levels.

The energies of crystal field levels of Nd^{3+} multiplets relevant to laser operation, determined from low-temperature absorption and emission spectra are gathered in Table 3. The $^4F_{3/2}$ multiplet splitting was found to be 244 cm^{-1}, a value about 3 times higher than that for Nd:YAG system. The overall $^4I_{11/2}$ splitting of 670 cm^{-1} is markedly bigger than 519 cm^{-1} reported for Nd:YAG.

Fig. 4 shows room temperature emission spectra related to the $^4F_{3/2} \rightarrow {}^4I_{11/2}$ and $^4F_{3/2} \rightarrow {}^4I_{13/2}$ transitions calibrated in the cross section units. To perform the calibration the calculated values of

Table 2
Calculated values of the radiative transition rates W_r and branching ratios β for the $^4F_{3/2}$ level of Nd^{3+} in CaF_2.

Transition from the $^4F_{3/2}$ level to level indicated	Transition wavelength [nm]	W_r [s^{-1}]	β
$^4I_{9/2}$	881	203	0.26
$^4I_{11/2}$	1083	466	0.60
$^4I_{13/2}$	1380	99	0.13
$^4I_{15/2}$	1924	4	0.01

$\sum W_r$ [s^{-1}] = 772; $\tau_{rad}(^4F_{3/2})$ = 1295 μs.

Table 3
Energies of the crystal field levels of the $^4I_{9/2}$, $^4I_{11/2}$, $^4I_{13/2}$ and $^4F_{3/2}$ multiplets of Nd^{3+} in CaF_2 crystal.

SLJ manifold	Energy [cm^{-1}]
$^4I_{9/2}$	0, 153, 301, 493, 790
$^4I_{11/2}$	1788, 1967, 2156, 2198, 2346, 2458
$^4I_{13/2}$	7129, 7244, 7399, 7454, 7494, 7570, 7672
$^4F_{3/2}$	11,339, 11,583

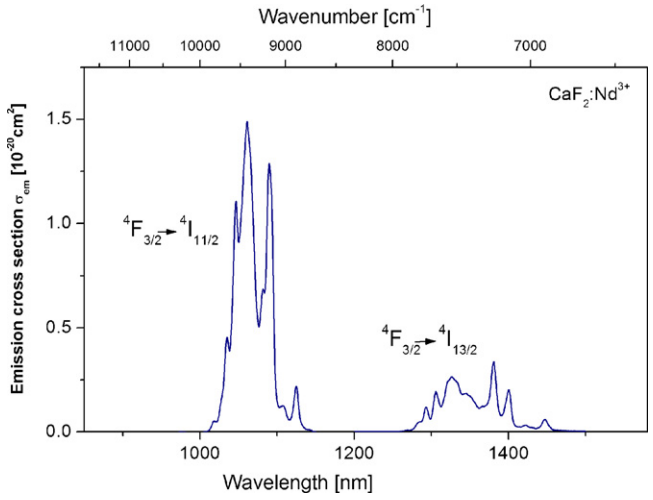

Fig. 4. The emission cross-sections of the $^4F_{3/2} \rightarrow {}^4I_{11/2}$ and $^4F_{3/2} \rightarrow {}^4I_{13/2}$ transitions of Nd^{3+} in CaF_2.

the radiative lifetime and branching ratio were inserted into the Fuchtbauer–Ladenburg relation, i.e.

$$\sigma_{em}(\lambda) = \frac{\beta\lambda^5}{8\pi c n^2 \tau_{rad}} \times \frac{I(\lambda)}{\int I(\lambda)\lambda\, d\lambda},$$

where β is the branching ratio (for $^4F_{3/2}$ level, $\beta = 1$), and $I(\lambda)$ represents the experimental emission intensity as a function of the wavelength λ.

The evaluated peak emission cross-section values for these transitions are 1.48×10^{-20} cm^2 at 1061 nm, and 0.34×10^{-20} cm^2 at 1380 nm, respectively. For a comparison the reported values of the peak emission cross section for other Nd^{3+}-doped fluoride crystals are: 1.7×10^{-20} cm^2 at 1036 nm and 0.4×10^{-20} cm^2 at 1.3 μm [28] in Nd-doped SrF_2 crystal, $0.4–0.5 \times 10^{-20}$ cm^2 at 1.3 μm in Nd-doped SrF_2–CaF_2 disordered crystal [33], 6.1×10^{-20} cm^2 at 1.05 μm and 1.5×10^{-20} cm^2 at 1.35 μm in

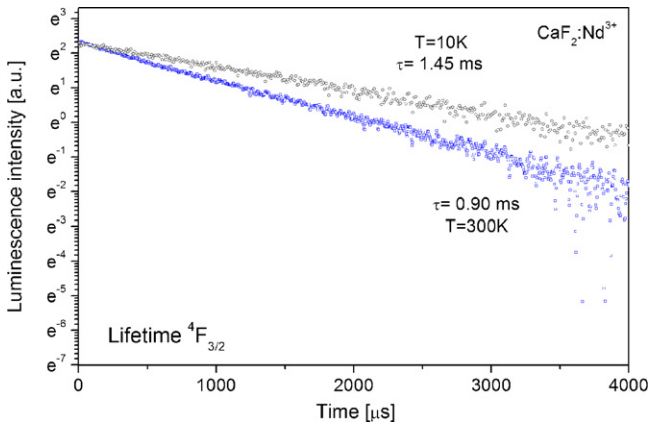

Fig. 5. Semi-log plots of CaF_2:0.75 wt% Nd^{3+} luminescence decay curves recorded at 10 K and 300 K.

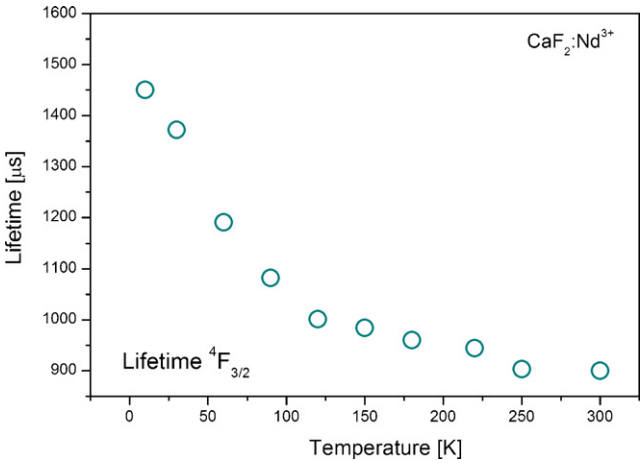

Fig. 6. The $^4F_{3/2}$ lifetime versus temperature for CaF_2:0.75 wt% Nd^{3+}.

Nd-doped ScF_3–CaF_2 disordered crystal [34], 1.98×10^{-20} cm^2 at 1049 nm and 0.49×10^{-20} cm^2 at 1.3 μm in Nd-doped GdF_3–CaF_2 disordered crystal [35]. It may be interesting to notice that the emission spectrum of Nd:CaF_2 system contains a narrow line at 1090 nm having the peak cross section of 1.29×10^{-20} cm^2, thus offering a possibility of lasing at 1090 nm.

The $^4F_{3/2}$ luminescence decay curves for Nd:CaF_2 were recorded as a function of the temperature from 10 K to 300 K. Fig. 5 compares the luminescence decay curves of Nd:CaF_2 recorded at 10 K and 300 K. They follow single-exponential time dependencies with different time constants amounting to 1.45 ms at 10 K and 0.90 ms at 300 K. With the temperature increasing from 10 K to 300 K, the luminescence lifetime values decrease monotonically (as shown in Fig. 6).

Data shown in Figs. 5 and 6 indicate unambiguously that a temperature-dependent process contributes to the $^4F_{3/2}$ decay. We think there are mainly three factors effecting on the nonradiative transition rate of Nd^{3+} $^4F_{3/2}$ manifold state in the crystal. They are the energy transfer from the Nd^{3+} ions to the structure defects (i.e. F_i^-, V_{Ca}), the interaction between Nd^{3+} ions in Nd–Nd clusters, and the multiphonon relaxation arose from the interaction between the Nd^{3+} ions and the fluctuating crystalline electric field due to the vibrations of Ca–F bands, respectively.

With the temperature increasing, the vibrations of atoms will be enhanced, and the formation of defects will be promoted. As a result, the interaction between the Nd^{3+} ions and that between Nd^{3+} ions and crystalline electric field will be potentiated. So, the multiphonon relaxation process will be intensified, and the nonradiative transition rate of Nd^{3+} $^4F_{3/2}$ level will increase. As far as know, the phenomenon of the self-quenching of luminescence in Nd:CaF_2 system has not been studied before and it is worth considering in future works.

4. Conclusions

High optical quality Nd-doped CaF_2 crystal was obtained by TGT method. The segregation coefficient of Nd^{3+} ion was about 0.82 in CaF_2 host crystal. At 300 K, both the pump band near 791 nm and emission band near 1061 nm are advantageously broad. Peak absorption cross-section of the $^4I_{9/2} \rightarrow {}^4F_{5/2}$ transition was 0.75×10^{-20} cm^2 at 791 nm, and the peak emission cross-sections of the $^4F_{3/2} \rightarrow {}^4I_{11/2}$ transition was 1.48×10^{-20} cm^2 at 1061 nm. The $^4F_{3/2}$ luminescence lifetimes with 1.45 ms at 10 K and 0.90 ms at 300 K were determined from luminescence decay curves. The $^4F_{3/2}$ radiative lifetime was calculated to be 1295 μs and the luminescence branching ratio of $^4F_{3/2} \rightarrow {}^4I_{11/2}$ laser transition was 60%. All

these spectroscopic parameters combined with an advantageously broad and intense absorption band near 791 nm indicate that the Nd:CaF_2 system is a promising active material for the design of laser-diode pumped infrared lasers.

Acknowledgements

The authors are indebted to the National Science Foundation of China (Grant No. 60938001, No. 60908030), the National High Technology Research and Development Program of China (Grant No. 2009AA03Z435) and the Science and Technology Commission of Shanghai Municipality (Grant No. 09JC1415300).

References

[1] A.A. Kaminskii, L.S. Kornienko, A.M. Prokhorov, Sov. Phys. JETP 21 (1965) 318.
[2] A.A. Kaminskii, L.S. Kornienko, L.V. Makarenko, A.M. Prokhorov, M.M. Fursikov, Sov. Phys. JETP 19 (1964) 262.
[3] A.A. Kaminskii, JETP Lett. 6 (1967) 115.
[4] A.A. Kaminskii, V.V. Osico, A.M. Prochoro, Yu.K. Voronko, Phys. Lett. 22 (1966) 419–421.
[5] T.P.J. Han, G.D. Jones, R.W.G. Syme, Phys. Rev. B 47 (1993) 14706–14723.
[6] T.T. Basiev, A.Ya. Karasik, V.V. Fedorov, K.W.Ver. Steeg, J. Exp. Theor. Phys. 86 (1998) 156–163.
[7] T.T. Basiev, V.V. Fedorov, A.Ya. Karasik, K.K. Pukhov, J. Lumin. 81 (1999) 189–197.
[8] Y.V. Orlovskii, T.T. Basiev, V.V. Osiko, H. Gross, J. Heber, J. Lumin. 82 (1999) 251–258.
[9] Y.V. Orlovskii, V.V. Fedorov, T.T. Basiev, M. Altwein, B. Leu, J. Heber, S. Mirov, J. Lumin. 83–84 (1999) 361–366.
[10] V.V. Fedorov, W. Beck, T.T. Basiev, Ya.A. Karasik, C. Flytzanis, Chem. Phys. 257 (2000) 275–281.
[11] D.K. Sardar, R.C. Velarde-Montecinos, S. Vizcarra, Phys. Stat. Sol. (a) 136 (1993) 555–560.
[12] H. Tanaka, N. Kawaguchi, N. Abe, Y. Furuya, Y. Yokota, T. Yanagida, J. Pejchal, M. Nikl, Y. Kawazoe, A. Yoshikawa, Opt. Mater. 33 (2011) 284–287.
[13] Z.G. Xia, P. Du, J. Mater. Res. 25 (2010) 2035–2041.
[14] G. Buse, E. Preda, M. Stef, I. Nicoara, Phys. Scripta 83 (2011) 025604.
[15] M. Siebold, M. Hornung, S. Bock, J. Hein, M.C. Kaluza, J. Wemans, R. Uecker, Appl. Phys. B 89 (2007) 543–547.
[16] T. Toepfer, J. Neukum, J. Hein, M. Siebold, Laser Focus World, 46, October 1, 2010.
[17] Z. Lin, X.L. Liang, Y.W. Ou, C.X. Fan, S.L. Yuan, H.D. Zeng, G.R. Chen, J. Alloys Compd. 496 (2010) L333.
[18] W. Saito, I. Ikejima, Y. Fukuda, Y. Momoi, Radiat. Meas. 46 (2011) 286–291.
[19] H. Lin, D.Q. Chen, Y.L. Yu, Z.F. Shan, P. Huang, A.P. Yang, Y.S. Wang, J. Alloys Compd. 509 (2011) 3363–3366.
[20] P. Samuel, H. Ishizawa, Y. Ezura, K.I. Ueda, S.M. Babu, Opt. Mater. 33 (2011) 735–737.
[21] S. Renard, P. Camy, A. Braud, J.L. Doualan, R. Moncorge, J. Alloys Compd. 451 (2008) 71–73.
[22] F.A. Bolshchikov, E.A. Garibin, P.E. Gusev, A.A. Demidenko, M.V. Kruglova, M.A. Krutov, A.A. Lyapin, I.A. Mironov, V.V. Osiko, V.M. Reiterov, P.A. Ryabochkina, N.V. Sakharov, A.N. Smirnov, S.N. Ushakov, P.P. Fedorov, Quantum Electron. 41 (2011) 193–197.
[23] S. Khiari, M. Velazquez, R. Moncorge, J.L. Doualan, P. Camy, A. Ferrier, M. Diaf, J. Alloys Compd. 451 (2008) 128–131.
[24] C. Pandurangappa, B.N. Lakshminarasappa, B.M. Nagabhushana, J. Alloys Compd. 489 (2010) 592–595.
[25] J.W. Ye, Y. Liu, Z.W. Zhao, Z.T. Jiang, Z.H. Tang, J. Alloys Compd. 496 (2010) 278–281.
[26] W.G. Liu, X.B. Liu, Z.G. Zhang, J. Guo, J. Alloys Compd. 470 (2009) L225.
[27] C.B. Huang, L.Z. Du, W.G. Zhang, J. Alloys Compd. 479 (2009) 777–784.
[28] S.A. Payne, J.A. Caird, L.L. Chase, L.K. Smith, N.D. Nielsen, W.F. Krupke, J. Opt. Soc. Am. B 8 (1991) 726–740.
[29] B.R. Judd, Phys. Rev. 127 (1962) 750–761.
[30] G.S. Ofelt, J. Chem. Phys. 37 (1962) 511–520.
[31] W.T. Carnall, P.R. Fields, K. Rajnak, J. Chem. Phys. 49 (1968) 4424.
[32] D.Q. Chen, Y.S. Wang, Y.L. Yu, E. Ma, F. Liu, J. Phys. Chem. Solids 68 (2007) 193–200.
[33] V.B. Sigachev, T.T. Basiev, M.E. Doroshenko, V.V. Osiko, A.G. Papashvili, OSA Technical Digest Series 18 (1995), ThD6/52-55.
[34] A.A. Kaminskii, Z.I. Zhmurova, V.A. Lomonov, S.E. Sarkisov, Phys. Stat. Sol. (a) 84 (1984) K81.
[35] A.A. Kaminskii, N.R. Agamalyan, G.A. Denisenko, S.E. Sarkisov, P.P. Fedorov, Phys. Stat. Sol. (a) 70 (1982) 397–406.